nature energy

Article

https://doi.org/10.1038/s41560-024-01458-1

Hydrogen storage and geo-methanation in a depleted underground hydrocarbon reservoir

Received: 1 September 2022

Accepted: 8 January 2024

Published online: 16 February 2024

Check for updates

Cathrine Hellerschmied[1,2,5], Johanna Schritter[1,5], Niels Waldmann[1], Artur B. Zaduryan[1], Lydia Rachbauer[3], Kerstin E. Scherr[1], Anitha Andiappan[4], Stephan Bauer[4], Markus Pichler[4] & Andreas P. Loibner[1]

Coupling of power-to-gas processes with underground gas storage could effectively allow surplus electricity to be stored for later use. Depleted hydrocarbon reservoirs could be used as stores, but practical experience of hydrogen storage in such sites is limited. Here we present data from a field trial that stored 119,353 m^3 of hydrogen admixed to natural gas in a depleted hydrocarbon reservoir. After 285 days, hydrogen recovery was 84.3%, indicating the process's technical feasibility. Additionally, we report that microbes mediated hydrogen conversion to methane. In laboratory experiments studying mesocosms that mimic real reservoirs, hydrogen and carbon dioxide were converted to methane (0.26 mmol l^{-1} h^{-1} evolution rate) reproducibly over 14 cycles in 357 days. This rate theoretically allows 114,648 m^3 of methane per year to be produced in the test reservoir (equivalent to ~1.08 GWh). Our research demonstrates the efficiency of hydrogen storage and the importance of geo-methanation in depleted hydrocarbon reservoirs.

Achieving net-zero carbon emissions by 2050 will require extensive electrification and broad deployment of renewable energy technologies[1], which produce intermittent surplus electricity from naturally fluctuating renewable resources such as solar or kinetic energy of wind[2]. In the Northern Hemisphere, peak renewable energy generation during summer is decoupled from peak energy consumption, typically in winter[2,3]. To retain surplus energy generated during peak production periods, we require solutions for high-capacity cross-seasonal storage of electrical energy currently unavailable due to technological and economic constraints[4,5].

Power to gas is a promising concept to retain surplus renewable energy by transforming electricity into chemical energy[6–8]. Power to gas uses renewable electrical energy for water electrolysis, generating gaseous energy carriers such as green hydrogen (H_2)[9] or methane (CH_4). These gases can then be injected into the natural gas grid[10]. Depleted hydrocarbon reservoirs (DHRs) have been proposed for large-scale cross-seasonal storage of gaseous energy carriers, thus reinforcing energy grid stability[11]. The potential of H_2 storage in DHRs has been theoretically explored since the late 1970s[12,13]. However, to date, practical experience with the storage of H_2 in the subsurface remains very limited. H_2-rich mixtures have been stored in salt caverns and saline aquifers[14,15] with only a single reported instance of H_2 storage in a DHR at a low pressure[16]. It remains unclear whether H_2 may affect the long-term stability and integrity of the reservoir (for example, via chemical reactivity with the brine and the reservoir rock). Moreover, H_2 storage and utilization may be compromised by the incompatibility of natural gas infrastructure with higher concentrations of H_2 in the gas mix[17]. Apart from H_2 storage, several studies have explored the microbial

[1]Institute of Environmental Biotechnology, Department of Agrobiotechnology IFA-Tulln, BOKU, University of Natural Resources and Life Sciences, Vienna, Austria. [2]Division of Microbial Ecology, Center for Microbiology and Ecosystem Science, University of Vienna, Vienna, Austria. [3]Biological Systems and Engineering Division, Lawrence Berkeley National Laboratory, Berkeley, CA, USA. [4]RAG Austria AG, Vienna, Austria. [5]These authors contributed equally: Cathrine Hellerschmied, Johanna Schritter. e-mail: andreas.loibner@boku.ac.at

conversion of H_2 to CH_4 in the presence of carbon dioxide (CO_2) in DHRs[18,19]. The use of DHRs for bio-methanation, hereby referred to as geo-methanation, is thought to play a vital role in a renewable energy future[20]. Unlike H_2, CH_4 is fully compatible with the existing energy infrastructure. It is three times higher in energy density per unit volume than H_2, which is critically advantageous for some industrial processes such as steel or cement production[21].

Geo-methanation provides notable advantages compared to established biological CH_4 production technologies, such as biogas upgrading[22,23], including reduced land use and the vast reaction volume provided by DHRs. At the same time, geo-methanation has possible limitations. Like any power-to-fuel process, methanation is associated with an inevitable loss of energy[24–26]. Not every reservoir may be suitable for geo-methanation because low porosity, water saturation, temperature, pH and high salt concentrations may limit and inhibit microbial activity and thus the conversion of H_2 to CH_4[24].

$$4H_2 + HCO_3^- + H^+ \leftrightarrow CH_4 + 3H_2O \quad (1)$$

$$4H_2 + SO_4^{2-} + H^+ \leftrightarrow HS^- + 4H_2O \quad (2)$$

$$4H_2 + 2HCO_3^- + H^+ \leftrightarrow CH_3COO^- + 4H_2O \quad (3)$$

$$CH_3COO^- + H_2O \leftrightarrow CH_4 + HCO_3^- \quad (4)$$

Hydrogenotrophic methanogenesis, the biological conversion of H_2 and CO_2 to CH_4 (equation (1)), is mediated by a diverse metabolic group of microbes known as methanogens[27,28]. Methanogens are critical players in established biotechnological and industrial processes, such as anaerobic wastewater treatment or biogas production from organic waste[29]. However, different microbial groups typically inhabit DHRs and mediate biochemical reactions with H_2 as electron donor. Homoacetogens and sulfate-reducing bacteria (SRB) are the most noteworthy groups competing for H_2 to produce acetic acid and hydrogen sulfide (H_2S), respectively (equations (2) and (3))[30,31]. Any conditions under which either group[32] outcompetes methanogens, for example, at low pH or when sulfate (SO_4^{2-}) is present in excess, could prove detrimental to H_2 storage and geo-methanation alike. Accumulation of acetic acid translates into product loss and acidification of reservoir brine, which could negatively impact methanogenesis and the integrity of the reservoir. Microbial sulfate reduction may result in the production of H_2S, a toxic gas harmful to health and infrastructure due to its corrosive effect on concrete and carbon steel[33].

Here we investigate the technical feasibility of natural gas and H_2 co-storage in a field trial across seasons in a real DHR. Using stable isotope and gas analysis, we provide evidence of active geo-methanation in the DHR, triggered by providing H_2 to the native microbial community at pressures up to 78 bar and a temperature of 40 °C. Laboratory-based experiments with reservoir-mimicking mesocosms, online pressure monitoring, gas composition analysis and molecular methods demonstrate that geo-methanation is a complete, rapid and stable process.

Hydrogen migration and recovery in DHRs

The Underground Sun Storage project[34] conducted the co-storage of natural gas (Supplementary Table 1) and H_2 (9.9% (v/v)) at high pressures in a DHR named Lehen (48° 01′ 45.0″ N 13° 41′ 29.6″ E, Unterpilsbach, Austria), further referred to as the test reservoir (Supplementary Fig. 1). This cross-seasonal field trial comprised three distinct phases: injection, where gas is introduced into the reservoir, leading to an increase in pressure; shut-in, where gas is sealed and stored in the reservoir until the onset of the last phase; and production, where gas is extracted from the reservoir. The injection of 1,206,802 m^3 of natural gas/H_2 mixture over 96 days was followed by a shut-in spanning 112 days, after which a larger gas volume of 1,299,997 m^3 was withdrawn over 76 days.

We successfully recovered 84.3% of the injected H_2 (Supplementary Table 2). Potential causes for the incomplete H_2 recovery could be either physico-chemical or biological. These may include escape from the reservoir through undetected leaks, dissolution in brine, chemical reactions with minerals and brine, migration to distant regions of the reservoir caused by diffusive and dispersive forces and microbial H_2 consumption by homoacetogens, sulfate reducers and methanogens.

The tightness of the cap rock is a primary concern for subsurface H_2 storage. Historically, DHRs have been successfully utilized as storage facilities for natural gas due to their ability to safely contain its main constituent, CH_4, over time at high pressures[33]. Recent studies have shown that effective permeability for representative cap rock samples (Hall formation) is of the same order of magnitude for H_2 ($2.3–2.7 \times 10^{-18}$ m^2) and CH_4 ($2.1–2.5 \times 10^{-18}$ m^2) (ref. [35]).

Hydrogen dissolution in brine is another potential explanation for the observed H_2 loss. Although the solubility of H_2 is slightly lower in brine than in pure water, it is within the same order of magnitude[36]. On the basis of H_2 solubility in brine under reservoir conditions (78 bar and 40 °C) (ref. 36) and an estimated brine volume of 40,000 m^3 in the test reservoir, the volume of dissolved H_2 should not exceed 3,692 m^3. This accounts for roughly 3% of the injected H_2 and thus cannot explain the incomplete H_2 recovery.

The chemical reactivity of H_2 may lead to mineral dissolution and alteration of the brine composition, thus potentially reducing H_2 recovery. Previous studies discussed the risk of H_2-mediated redox reactions with carbonate, iron-bearing and sulfur-bearing minerals[37–39] and carbonates or sulfates dissolved in brine[12,13] in the context of underground H_2 storage. The chemical reduction of sulfates and other sulfur species with H_2 results in the generation of H_2S, a highly corrosive and toxic gas, decreasing the quality of the stored gas and potentially corroding the well material. Furthermore, calcite dissolution in the reservoir would reduce the stability of the reservoir grain structure and translate to increased sand production from the reservoir. However, we did not observe increased sand production (Supplementary Note 1), and H_2S was below the detection limit during shut-in and production (Supplementary Fig. 2). These findings are further corroborated by the results of geochemical experiments in which representative sandstone samples were exposed to CH_4/H_2-bearing gas mixtures (25% and 75% of H_2) at reservoir conditions for 357 days and tested for change in flow parameters, permeability and grain structure[34]. Their results showed no H_2-induced changes in reservoir rock material, suggesting no mineral dissolution occurred throughout the H_2 storage field trial. Together, these findings indicate that H_2 is unlikely to react with the reservoir rock or brine at storage site conditions over the evaluated time.

In porous rock, diffusion and dispersion will lead to gas mixing (Supplementary Note 2), which is probably the cause of H_2 flux into the cushion gas (natural gas present in the reservoir before the storage trial (Supplementary Table 3)). The trajectory of H_2 concentration across time informs on mixing dynamics during the field trial (Fig. 1a). At the beginning of gas withdrawal, the H_2 concentration was already lower than the average H_2 concentration during injection (9.84%; Fig. 1a, yellow horizontal line) and dropped continuously at increasing speed (Fig. 1b) as more gas was extracted from the reservoir (Supplementary Note 2). After the withdrawal of the entire injected volume (indicated by the red vertical line in Fig. 1b) and an additional 93,195 m^3 of cushion gas, we found a residual H_2 concentration of 2.8% (blue dashed horizontal), which indicates substantial migration of H_2 into the initially H_2-free cushion gas. Due to the system's complexity, it is very challenging to determine the exact volume of H_2 that migrated into the cushion gas. By employing a modified decline curve analysis (Supplementary Fig. 3 and 'Decline curve analysis' in Methods), we estimated that 9,310 m^3 of H_2 remained in the cushion gas, corresponding to 40% of the unaccounted H_2.

https://doi.org/10.1038/s41560-024-01458-1

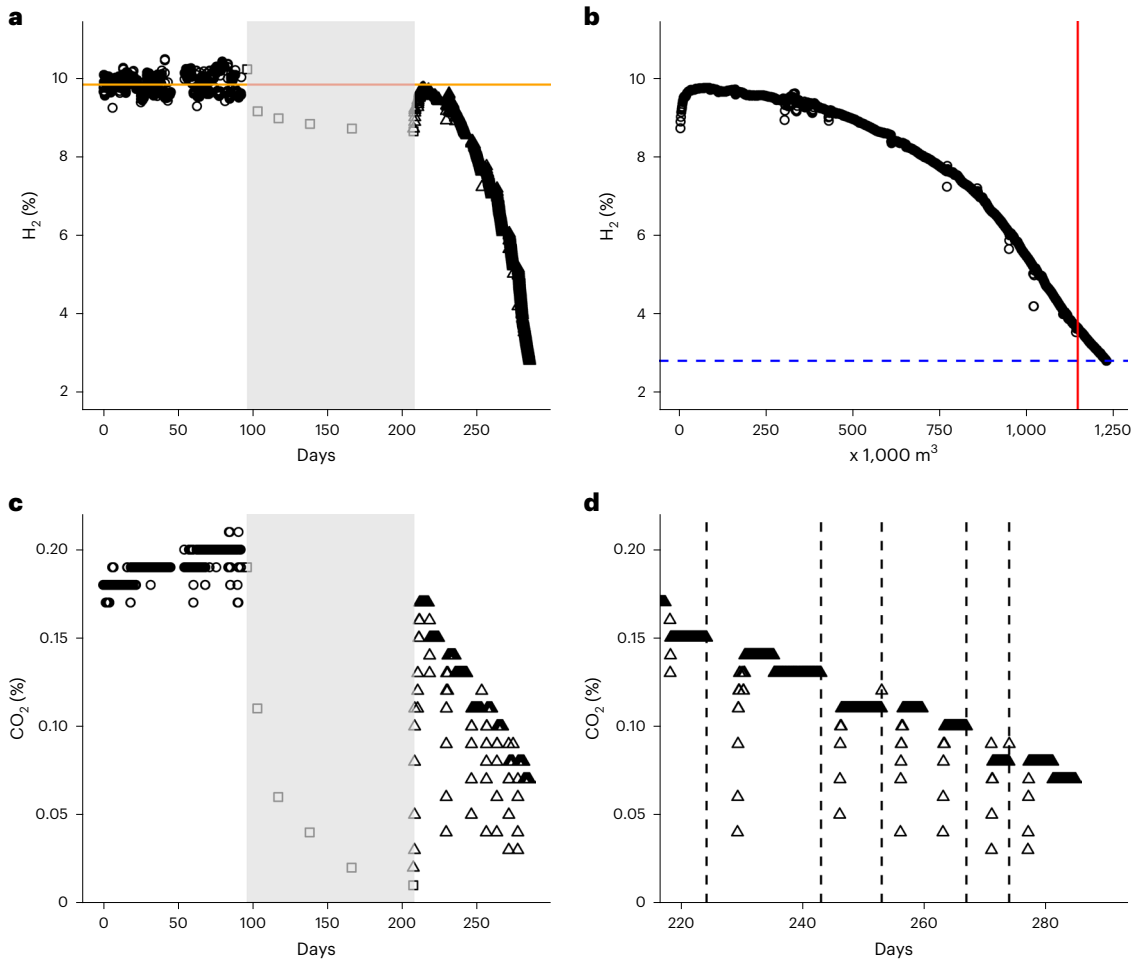

Fig. 1 | Change of H_2 and CO_2 concentrations during H_2 co-storage in the Lehen test reservoir. a, Monitoring of H_2 across one storage cycle comprising injection (circles), gas is pressed into the reservoir; shut-in (grey shading, squares), gas is sealed and stored in the reservoir; production (triangles), gas is produced from the reservoir. The yellow horizontal line indicates the mean H_2 concentration during injection. **b**, Zoom in on the H_2 concentration trajectory during the production phase. The red vertical line signifies the threshold beyond which the withdrawal of cushion gas took place. A dashed, blue horizontal line indicates the H_2 concentration at the end of the field trial. **c**, Monitoring of CO_2 concentration across all phases of the field trial. **d**, Zoom in on the CO_2 concentration trajectory during the production phase: CO_2 concentration drops following short breaks in gas production termed 'mini shut-ins'. A vertical dashed line indicates the beginning of each mini shut-in.

Microbial activity during geo-methanation in DHRs

In DHRs, three major functional groups of microbes, that is, SRB, homoacetogens and methanogens compete for H_2 as a growth substrate[31]. The metabolic activity of SRB will result in the production of H_2S (equation (2)). However, we did not detect H_2S in the produced gas, suggesting that no substantial microbially mediated sulfate reduction occurred. Phylogenetic analysis based on the gene coding for 16S ribosomal ribonucleic acid (16S rRNA) (16S analysis) showed that known sulfate and sulfur-reducing bacterial groups were generally at low relative abundance (<2%), which tended to decrease further throughout the field trial (Supplementary Fig. 4).

Both homoacetogenic bacteria and methanogenic archaea utilize H_2 and CO_2 (derived from the co-stored natural gas) to produce acetic acid and CH_4, respectively. Although the bacterial fraction of the microbial community decreased overall from 92.6% to 83.0%, a few amplicon sequence variants (ASVs) associated with genera involved in syntrophic acetate oxidation[40,41], fermentation[42–44] and acetogenesis[45] increased their relative abundance substantially (Supplementary Figs. 4 and 5). These relative abundance shifts (*Syntrophaceticus* 31.5%, *Soehngenia* 11.2%, *Candidatus* Caldatribacterium 9.5%, *Acetoanaerobium* 3.5%) indicate that the bacterial community contributed to acetate cycling through acetate formation by fermentative and homoacetogenic species (most classified as Firmicutes; Supplementary Fig. 5) and syntrophic acetate oxidation-mediated oxidation of acetate to produce H_2 and CO_2. Although formation and cycling of acetate appear to play a role as an intermediate, the low concentration of acetate in the system upon completion of the field trial (102 mg l^{-1}) is well in line with concentrations reported for DHRs that have not been exposed to H_2 (Supplementary Table 4), suggesting that losses through acetate formation are small.

16S analysis revealed a twofold increase in the relative abundance of known methanogenic genera throughout the field trial from 7.3% to 17.0% (Fig. 2a). Furthermore, they account for a striking 61% of the active community during the production phase (Fig. 2b), corroborating the dominance of this microbial group in the system.

Finally, amplicon sequencing targeting the *mcrA* gene transcript encoding the α subunit of the methyl coenzyme M reductase, an established marker for methanogenesis[19,46], confirmed specific methanogenic activity in the reservoir (Supplementary Fig. 6). Sequence analysis of the *mcrA* and the 16S rRNA transcripts suggests that most active methanogens belong to the family Methanobacteriaceae (Fig. 2a–c), a group of strictly hydrogenotrophic methanogens that utilize H_2 to reduce CO_2[47]. These data imply that hydrogenotrophic

https://doi.org/10.1038/s41560-024-01458-1

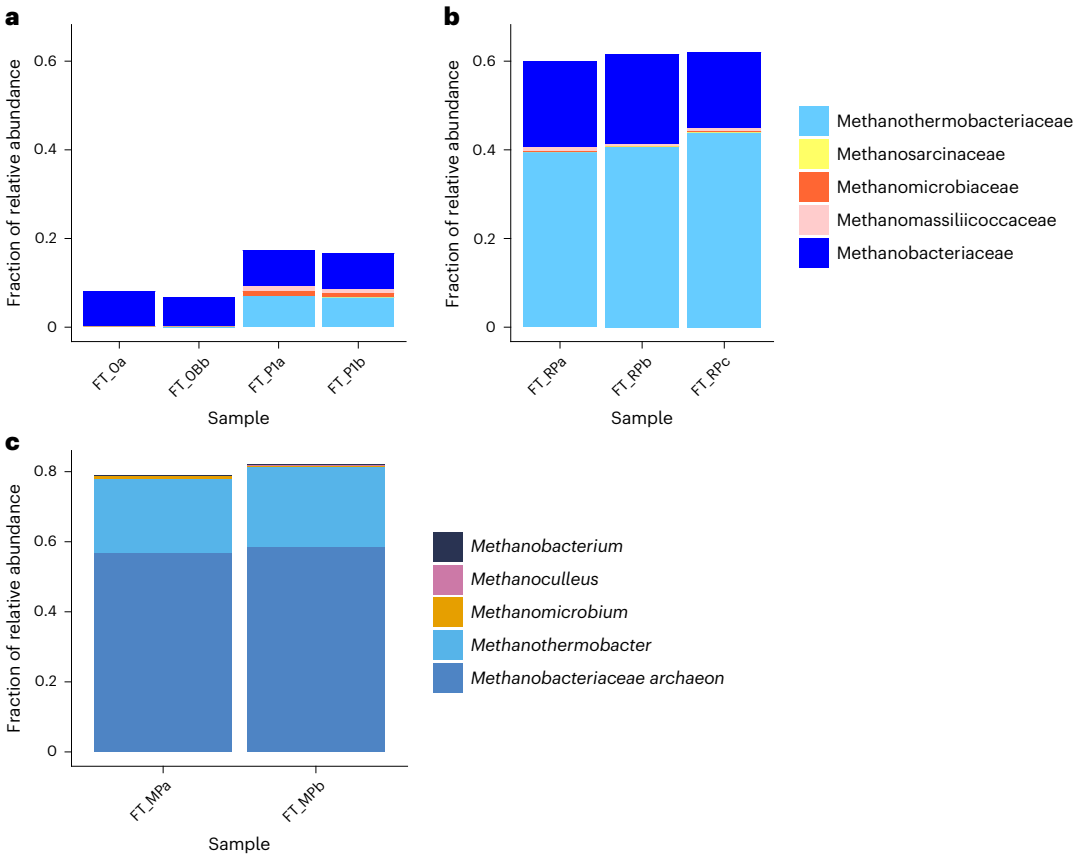

Fig. 2 | Relative abundance shifts and activity of methanogens in reservoir brine in response to H_2 co-storage. a, 16S rRNA gene-based relative abundance of members of the methanogenic community shown as duplicates at family level before storage (FT_0a, FT_0b) and on day 244 of the production phase (FT_P1a, FT_P1b) of the H_2 co-storage field trial ($n = 2$). **b**, Depicts the fraction of active methanogens (family level) in total community derived from total RNA isolated from brine sampled at day 244 of the production phase (FT_RPa, FT_RPb, FT_RPc) ($n = 3$). **c**, Relative abundance of methanogens based on *mcrA* marker gene transcripts (FT_MPa, FT_MPb) (genus level) of successfully amplified mRNA fragments, which were isolated from brine (day 244) ($n = 2$).

methanogens were initially present in the reservoir, increased in relative abundance throughout the field trial and actively performed methanogenesis. The extremely low abundances of acetoclastic methanogens (*Methanosaeta* and *Methanosarcina*, the only two genera known to perform acetoclastic methanogenesis; equation (4)) suggest a low direct acetate oxidation by methanogens[40].

The CO_2 balancing (Supplementary Table 5) showed that 960 m^3 of CO_2 was consumed throughout the field trial. Gas chromatographic analysis of samples drawn during shut-in (between days 96 and 207) shows an 87.4% decrease in CO_2 (Fig. 1c). Data from the subsequent gas production phase reveal two patterns: first, the gradual reduction of CO_2 concentrations with ongoing gas production suggests active geo-methanation in the reservoir (Fig. 1c). Second, a sharp drop in CO_2 concentration after short breaks in gas extraction (Fig. 1d) indicates high rates of CO_2 consumption in the near-wellbore region, defined as the reservoir volume within a 10 m radius around the wellbore. The CO_2 concentration remained low (<0.04%) after the completion of the field trial (Supplementary Table 6), indicating ongoing CH_4 formation by methanogenic archaea at the expense of H_2, which migrated into the cushion gas.

Dissolution of CO_2 into reservoir brine is another potential cause for the observed decrease of CO_2 concentrations. This is unlikely for the field trial as the CO_2 concentrations of the natural gas initially present in the reservoir (cushion gas) and the injected gas mixture are almost equal (0.22% and 0.19%, respectively). Gas withdrawal from the reservoir decreases reservoir pressure, which decreases CO_2 solubility and releases dissolved CO_2 into the gas phase rather than the observed reduced levels.

Stable carbon isotope analysis captures shifts in the isotope ratio ($^{13}C/^{12}C$) and points towards a biological origin of CH_4, specifically during the shut-in and production phase. Metabolic processes enrich the lighter ^{12}C isotope in the product, which manifests in a shift to a more negative isotope signature in products over time[48,49]. Hence, geo-methanation will decrease the CH_4 carbon isotope signature ($\delta^{13}C_{CH4}$; Fig. 3) in the reservoir. The average $\delta^{13}C_{CH4}$ signature reduced significantly from the injection to the production phase by 2.7 ± 0.5‰ (standard error; p value = 0.0002; $n = 11$, $n = 7$, respectively), suggesting a microbial origin for a fraction of the recovered CH_4. It must be noted that this overall shift could potentially be an artefact of the mixing of the injected CH_4 ($\delta^{13}C_{CH4}$: −56.8 ± 0.3‰) with cushion gas ($\delta^{13}C_{CH4}$: −61.6 ± 0.1‰).

During the 96-day injection, cushion gas is constantly driven deeper into the reservoir. This creates a zone around the wellbore accommodating only injected gas unaffected by the cushion gas' low carbon isotope signature. Hence, the significant shift of −3.8‰ ± 0.4‰, (standard error; p value = 0.0004) to a lighter $\delta^{13}C_{CH4}$ signature observed during shut-in (between samples taken at day 96 and day 166) supports the hypothesis of biological geo-methanation. These findings align with the observed CO_2 consumption near the wellbore and confirm the notion that this area exhibits considerable geo-methanation activity.

Efficiency of geo-methanation in DHR-simulating mesocosms

To explore geo-methanation under near-optimal conditions, we performed laboratory-based experiments in reservoir-mimicking

https://doi.org/10.1038/s41560-024-01458-1

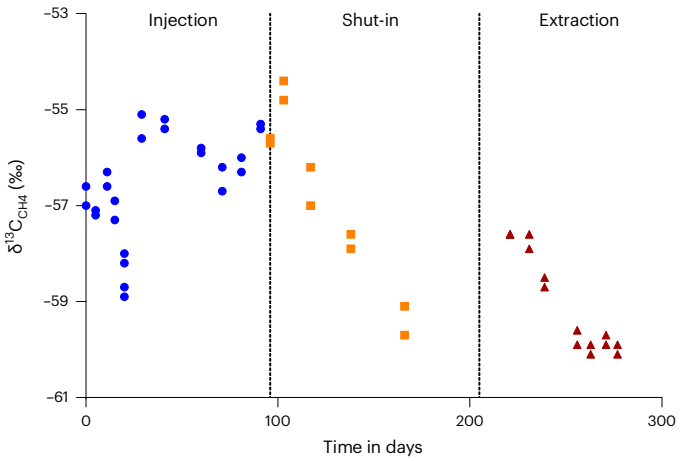

Fig. 3 | Change of stable carbon isotope ratios during H_2 co-storage in the Lehen test reservoir. $\delta^{13}C_{CH4}$ signature (‰; δ-notation according to Vienna Peedee Belemnite standard) measured during injection (circles), shut-in (squares) and production (triangles) phase of the field trial. Vertical dashed lines indicate the transition from injection to shut-in (left) and shut-in to production (right).

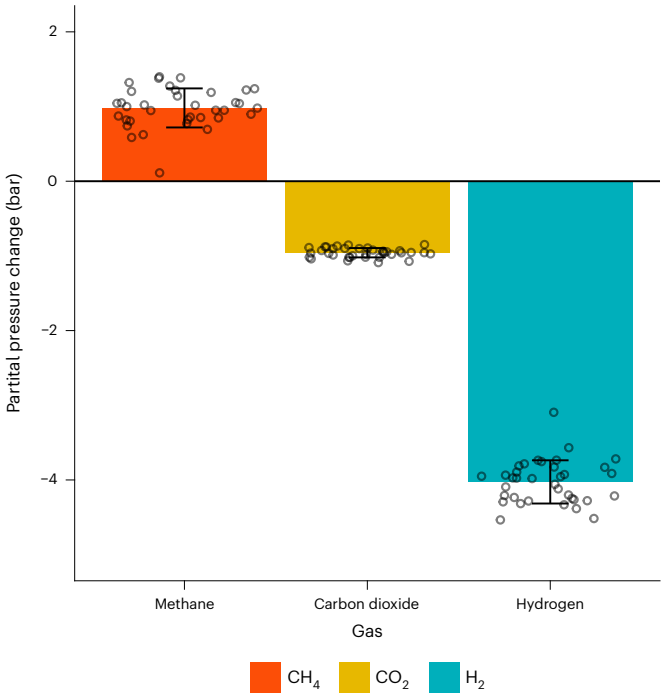

Fig. 4 | Changes in gas composition after geo-methanation in reservoir-mimicking mesocosm. Mean (bars) and individual partial pressure change (points) across substrate gas conversion cycles performed in the high-pressure mesocosm M1 ($n = 10$), M2 ($n = 10$) and M3 ($n = 22$), operated at an initial target pressure ($p0$) of 40 to 45 bar. Error bars represent the standard deviation from the mean. Data were corrected against abiotic sources of pressure loss as determined in abiotic control mesocosms M4 and M5.

mesocosms ('Mesocosm set-up' in Methods and Supplementary Fig. 7). Mesocosms (designated M1–M5) were loaded with representative sandstone cores, test reservoir brine, pressurized with a substrate gas mixture ($H_2/CO_2/CH_4$) and incubated at 40 °C and approximately 40 bar until the substrate gas was consumed. We repeatedly substituted the gas headspace in the mesocosms with fresh substrate gas to evaluate multiple sequential gas conversion cycles ($n = 10$ in M1 and M2, $n = 24$ in M3). We performed measurements of headspace gas composition at the start and end of each conversion cycle, except for two cycles in M3, where we took multiple intermediate gas samples to assess gas conversion kinetics (Supplementary Fig. 8). Across all cycles, substrate gases H_2 and CO_2 were converted to CH_4 at a stoichiometric ratio for H_2:CO_2 of 4:1 (Fig. 4). We observed no conversion in the abiotic controls (Supplementary Fig. 9).

In this study, we used pressure decline as a suitable proxy for the progression of the hydrogenotrophic methanogenesis. This conversion (equation (1)) is accompanied by a pressure loss, which results from the conversion of five moles of substrate gas (H_2 and CO_2) to one mole of the gaseous product (CH_4). To determine process stability and average conversion time, we performed multiple consecutive geo-methanation cycles in M3 and continuously monitored the pressure. Given the composition of the substrate gas mixture used in this experiment (10% (v/v) H_2 and 2.5% (v/v)) CO_2 in CH_4, we expected a total pressure loss of 10%. The normalized, average net pressure (0.906) converged almost perfectly to the expected value of 0.9, representing 90% residual pressure (Fig. 5a, orange line). Furthermore, the observed pressure decline in the biotic mesocosm aligns with the observed decrease in moles of H_2 (Supplementary Fig. 10). In contrast, the pressure in the abiotic mesocosms remained stable (Fig. 5a, grey line). Mesocosm pressure development was consistent across multiple cycles ($n = 14$) over 12 months (Fig. 5a, blue line).

To quantitatively assess the stability of substrate gas conversion, we defined two process metrics: the maximum H_2 consumption rate (CR_{max}) and the total pressure decrease (Δp) per conversion cycle ('Quantitative analysis of geo-methanation' in Methods). We found no significant change in CR_{max} (slope = −0.000015, p value = 0.541; Fig. 5b) or Δp (slope = 0.000007, p value = 0.550) over 357 days, which confirms long-term stability and robustness of the geo-methanation process under reservoir-mimicking conditions. Finally, we determined that, on average, 95% of the CH_4 production was completed within 4.9 days by intersecting the latent function[50] derived from pressure data of 14 conversion cycles with the constant at a relative pressure of 0.911 (Fig. 5a).

Using these results, we calculated the average CH_4 turnover rate (tr)[51] across all cycles in M3 to be 0.008 h^{-1} and found that it compares well to tr values obtained from investigations of hydrogenotrophic methanogenesis at high-pressure regimes using pure cultures[51,52]. The results presented here come remarkably close to the referenced study on *M. thermaggregans*, reporting a tr of 0.012 h^{-1} at H_2 partial pressure of 40 bar, given that the biomass concentration is probably lower in the mesocosms compared with pure culture cultivation in a medium designed to meet the requirements of methanogens.

In mesocosms M1 and M2, we investigated the effect of H_2 and CO_2 on the microbial community. In both cases, we sampled mesocosm fluids before substrate gas provision and after ten cycles of geo-methanation. The relative abundance of methanogens increased by 56% and 59% in M1 and M2, respectively (Fig. 6a), and methanogens represented almost 50% of the active microbial community (Fig. 6b) after ten conversion cycles performed over three months. Each cycle was paralleled by a pressure decline (Supplementary Fig. 11) indicative of the geo-methanation process and stoichiometric substrate gas depletion (Fig. 4 and Supplementary Data 1). Most methanogens contributing to the observed shift belong to the genus *Methanothermobacter*, which falls within the taxonomic group Methanobacteriaceae. Isolates of this group strictly utilize H_2 and CO_2 for energy generation[46] and are thus classified as hydrogenotrophic methanogens. *Methanothermobacter* abundance increased drastically and was identified as the most metabolically active player in the geo-methanation process for mesocosm trials. This aligns well with recent reports on *Methanothermobacter* species isolated from oil fields. It also shows the urgency of ongoing efforts to analyse the genome of hydrogenotrophic *Methanothermobacter* strains from oil fields[53,54]. We observed another sharp abundance increase for halophilic *Methanoculleus*, a type of hydrogenotrophic methanogen. These organisms syntrophically

https://doi.org/10.1038/s41560-024-01458-1

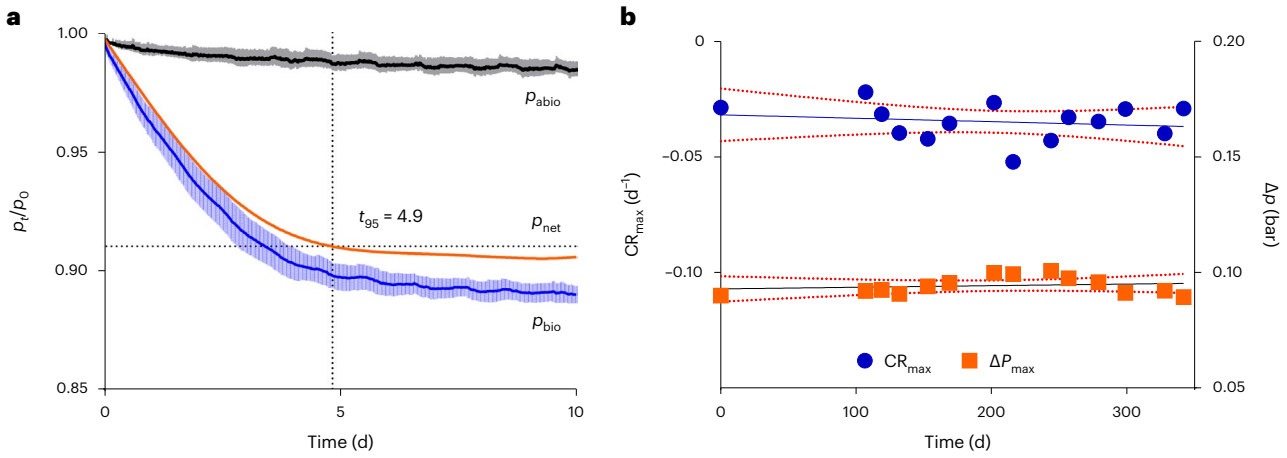

Fig. 5 | Gas conversion and pressure change in mesocosms. a, Normalized pressure progression in M3 (p_{bio}, blue line, $n = 14$) and across abiotic control mesocosms M4 and M5 (p_{abio}, grey line, $n = 3$ and $n = 7$, respectively). Data are presented as mean values ± SD. Gaussian fit (latent function) of net pressure loss of 14 conversion cycles performed in M3 (p_{net}, orange line, n per cycle = 481). The vertical dashed line denotes the intercept between the latent function and the benchmark of 95% of maximum theoretical pressure loss possible via geo-methanation (horizontal dashed line); t_{95} represents the average time to complete the geo-methanation cycle with a benchmark of 95% maximum pressure loss. p_t: mesocosm pressure at time point t; $p0$: initial mesocosm pressure. **b**, Linear regression of net pressure difference (Δp) and maximum conversion rate (CR_{max}) of 14 conversion cycles in M3. Red dotted lines show 95% confidence intervals of the regression line.

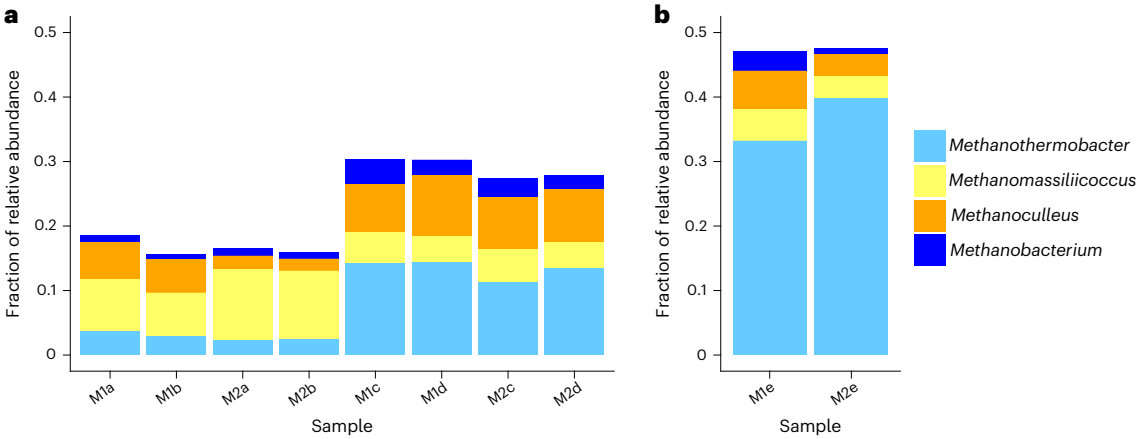

Fig. 6 | Relative abundance shifts of methanogens for mesocosm trials M1 and M2. a, 16S rRNA gene-based relative abundance of methanogenic community shown as technical duplicates at genus level before H_2/CO_2 provision (M1a/b, M2a/b) and after the tenth cycle of substrate gas conversion (M1c/d, M2c/d). **b**, RNA sequencing for both mesocosms M1 and M2 depicts the fraction of metabolically active methanogens (genus level) in the total community after ten gas conversion cycles (M1e, M2e).

generate CH_4 with acetate-oxidizing bacteria through the hydrogenotrophic pathway and are commonly found in marine and brackish environments[55]. Sequencing results align with gas composition and pressure data, suggesting that hydrogenotrophic methanogens are responsible for the observed geo-methanation under the reported conditions.

DHR geo-methanation under near-optimal conditions

On the basis of the result from laboratory-based mesocosm trials, DHRs could serve not only as cross-seasonal storage for renewable electricity in the form of H_2 but also for geo-methanation at large scale when CO_2 is co-injected with H_2. The potential of such a geo-methanation site lies in its vast storage capacity, representing the reaction space for converting stored H_2 and CO_2 to CH_4.

However, we observed considerable differences in geo-methanation performance between mesocosms and the field trial. We attribute these differences to several factors. First, in contrast to the field trial, the mesocosm experiments were conducted with a substrate gas mixture at optimal stoichiometry for hydrogenotrophic methanogenesis (mesocosms H_2:CO_2 = 4:1; field H_2:CO_2 = 52:1) to explore the process potential at near-optimal conditions. Second, the difference in scale of several orders of magnitude translates to greater heterogeneity of the environment for water saturation, porosity and gas permeability and unknown factors, which may have impeded the geo-methanation process in the field.

Assuming a similarly high and complete geo-methanation performance in the Lehen test reservoir as shown in mesocosms, the CH_4 yield per conversion cycle would amount to 27,170 Nm^3 (equation (8) and 'Methane evolution rate' in Methods) when operated at comparable conditions (10% H_2, 2.5% CO_2). However, implementing such a geo-methanation is constrained operationally by the time required for injection and production of gases (several months) rather than by microbial CH_4 formation (4.9 days for 95% conversion as calculated for mesocosms). Optimization of injection and production time could realistically allow up to four storage cycles per year for the test reservoir, increasing the potential annual CH_4 yield to 114,646 m^3 in this comparably small reservoir.

This volume corresponds to an energy content of roughly 1.08 GWh. Considering Europe's gas storage capacity (89 billion m^3 in DHRs)[52], geo-methanation could speed up the transition to a renewable energy system by providing a storable energy carrier compatible with the existing distribution and utilization infrastructure. One way to circumvent the downtime of injection and production would be a flow-through-like system where gases are continuously injected into one well, converted during passage through the reservoir with a residence time sufficient for complete conversion and produced at another well[56]. Such a mode of operation could substantially increase the CH_4 yield.

Productivity reported as methane evolution rate (MER) for pure cultures of various *Methanobacterium* species at an elevated pressure of 10 bar (ref. 52) compares well to the calculated average MER (equation (7)) of 0.26 mmol l^{-1} h^{-1} for the test reservoir operated at mesocosm productivity. At a MER as reported in this study, depleted natural gas reservoirs could serve as effective large-scale geo-methanation sites without the costly requirement of an external bioreactor, fermentation infrastructure and additional synthetic media.

A recent study showed that porous rocks and minerals beneficially influence the biological methanation of H_2 and CO_2[57]. As demonstrated in mesocosm M3 (Fig. 5b) using a porous sandstone core, CH_4 formation remained constant at a high level over 357 days and 14 cycles of repeated gas injection. These results underline the stability of geo-methanation and indicate suitability for belowground CH_4 production. Generally, results of geo-methanation experiments conducted in laboratory-based, reservoir-mimicking mesocosms suggest that DHRs have the potential to convert and store renewable energy in the form of green CH_4 at large scale, thus providing a drop-in fuel with existing infrastructure.

Conclusions

In summary, the results of this study suggest that overall DHRs are suitable for H_2 co-storage. The conversion of H_2 and CO_2 to CH_4 via geo-methanation could be an alternative route to store renewable energy. Because DHRs can differ substantially in several parameters[58] (that is, salinity, temperature, pH, pressure, microbial community composition) and thus in their potential geo-methanation performance, more research on the exact boundary conditions for H_2 co-storage and geo-methanation is required. Currently, the energy loss associated with geo-methanation is still unclear. Nevertheless, the unprecedented potential of 339 billion m^3 global gas storage volume in DHRs allows us to glimpse at the impact geo-methanation could have on a net-zero future energy system based on renewables.

Methods

Test reservoir

The depleted gas reservoir Lehen (Supplementary Fig. 1) served as the demonstration site for field testing. This isolated reservoir constitutes a porous 2-m-thick sandstone layer, part of the geological Hall formation within the Upper Austrian Molasse Basin[59]. The reservoir stretches about 16 hectares and is located 1,027 m below the surface (total vertical depth, TVD). The gas-accommodating porous sandstone layer is encased by a cap rock composed of clay minerals, thus preventing the gas from migrating into neighbouring geological layers. Like many other underground gas reservoirs explored in the Molasse Basin in Austria and Germany, the Lehen gas reservoir held biogenic natural gas[60]. This formation mainly consists of fluvial and shallow-marine sandstones, shales and carbonates[59]. Upon exploration, the reservoir exhibited an initial absolute pressure of 107 bar and a volumetric capacity of around 6,434,981 m^3 natural gas. The temperature in the reservoir is 40 °C.

Preparative action

We monitored the subsurface pressure development using two gauges (Sondex/Panex × $1^{11}/_{16}$′, OW-00175 and OW-00169; Canada Tech) installed in the wellbore at 1,012.81 m and 1,023.03 m TVD, respectively. Natural gas used in the field trial was conditioned according to the Austrian Gas Standard G31. The added H_2 (3.0) was purchased from Linde Gas GmbH.

Field trial operation

The field trial recreated a complete gas storage cycle over 285 days. A gas storage cycle comprises three phases: injection, shut-in and production. Injection and production denote the phases of pressing gas into (reservoir pressure increases) and extracting gas out (reservoir pressure decreases) of the reservoir. To avoid integrity issues, a natural gas reservoir is never fully depleted. This residual gas is termed 'cushion gas.'

In this field trial, we injected a gas volume of 1,206,802 m^3 containing CH_4 (88.6% (v/v)), H_2 (9.89% (v/v)), N_2 (0.5% (v/v)), C_2H_6 (0.45% (v/v)), CO_2 (0.19% (v/v)) and trace amounts of C_3–C_6 alkanes (<0.4% (v/v)) into the Lehen reservoir over 96 days and shut-in for 112 days. Before the field trial, the reservoir had contained only natural gas. During injection, the absolute pressure in the reservoir increased from 35.1 bar to 78.4 bar. After the shut-in, 1,299,997 m^3 of gas was produced from the reservoir within 76 days at a rate of 1,055 m^3 h^{-1}. To investigate the potential of H_2 migration into the cushion gas, the production volume exceeded the injected gas volume by 93,195 m^3, yielding a final absolute pressure of 28.3 bar. All volumetric values are given in standard m^3.

Field trial gas analysis

To allow monitoring of gas components, RAG Austria AG analysed field gases using a gas chromatograph (Siemens Maxum, columns: HAYESEP N 80/100, MOLSIEB 5 A 80/100, HAYESEP N100/120, 1.0% TCEP CARBOBLACK B 80/120), which was installed next to the wellhead. At this stage, the produced gas is untreated except for the elimination of free water, reflecting the gas composition in the reservoir. Besides the key analytes, H_2, CO_2 and CH_4, N_2, O_2, H_2S, ethane, propane, *i*-butane, *i*-pentane, *n*-butane, *n*-pentane, neo-pentane and hexane were quantified. The composition of the gas stream was monitored continuously during injection and production. During shut-in, gas samples were analysed at selected time points.

We estimated CO_2 and H_2 balances by calculating the difference in gas volumes (V) moving in and out of the reservoir according to equation (5), where ΔVj denotes the overall change of volume of the gas component j and Vc is the volume of component j in the excess cushion gas extracted during production. ∑Vji, ∑Vjp and ∑Vjs denote the sum of all discrete volumes of j calculated from the gas flow rate integrated over one hour and concentration of j during injection (i), production phase (p) and shut-in (s), respectively. All plots and calculations were done with custom-made R code.

$$\Delta Vj = Vcj + \sum Vji - \left(\sum Vjs + \sum Vjp\right) \quad (5)$$

Decline curve analysis

We approximated the amount of H_2 that has migrated into the cushion gas of the reservoir via a modified decline curve analysis[61]. The partial pressure of H_2 in the withdrawn gas was estimated with an exponential fit. The exponential decline profile was indicated by flow-through experiments[34]. The method does not consider the heterogeneity of the reservoir or the transition zone between the cushion gas and the H_2-bearing gas, which is not clearly defined. This could potentially lead to an underestimation of gas migration.

Compound-specific stable isotope analysis

Isodetect GmbH (Leipzig) determined carbon isotope ratios ($^{13}C/^{12}C$) of CH_4 through compound-specific stable isotope analysis (CSIA)[49]. CSIA was accomplished via (1) manual injection of gas samples using a

gas-tight syringe into the split/splitless injector of a gas chromatograph (GC, 7890 A Series; Agilent Technology USA); (2) compound-specific separation of target compounds at 35 °C using a CP-Porabond Q column (50 m × 0.32 mm × 5 µm; Varian); (3) combustion of target compounds to CO_2 molecules for carbon isotope analysis and (4) transfer of CO_2 into an isotope ratio mass spectrometer (MAT 253, Thermo Fisher Scientific). Authentic laboratory standards were used to identify target compounds and quality control of CSIA. Isotope ratios are expressed in the delta notation ($\delta^{13}C$) in agreement with international standards according to equation (6), where R_{sample} and $R_{standard}$ represent the $^{13}C/^{12}C$ ratio of the sample and the international standard, respectively[49].

$$\delta^{13}C\,(‰) = \left(\frac{R_{sample} - R_{standard}}{R_{standard}}\right) \quad (6)$$

Vienna Pee Dee Belemnite was used as a standard for carbon CSIA. Each sample was analysed at least twice. The total analytical uncertainty concerning accuracy and reproducibility was ≤0.6‰.

Drill cores used in mesocosm experiments

Drill cores (litharentic sandstone) from the Sierning natural gas field (Upper Austria) were employed in mesocosm experiments, mimicking the field's conditions. Sierning is a gas reservoir in the Imbricated Upper Puchkirchen Formation[59], part of the Upper Austrian Molasse Basin. The sandstones from the Sierning gas reservoir compare well to the sandstone at the field trial site ('Gas reservoir') concerning carbonate content, porosity, grain size and permeability. X-ray diffraction analysis was carried out by OMV Exploration and Production GmbH with a Bruker D8 Advance Powder X-Ray Diffractometer, according to Schultz 1964; ISO 9001:2008. X-ray diffraction data of cores is provided in Supplementary Table 7. The effective porosity of the cores ranged from 20% to 22%, which is typical for sandstone of porous natural gas reservoirs in the Molasse Basin. Cylindrical drill cores (diameter 0.1 m) were cut to a length of 0.2 m and used in mesocosm experiments as a proxy for reservoir rock.

Test reservoir sampling and brine acquisition

Reservoir brine was sampled during two campaigns; the first, 155 days before H_2 injection (initiation of H_2 injection is considered day 0) at 1,430 m measured depth and the second during the extraction phase of the field trial on day 244 at 1,200 m measured depth. Before each sampling event, at least 10,549 m^3 of gas was produced to ensure that the brine sampled from the wellbore tubing is representative of the reservoir. The tubing of the wellbore is perforated only at the level of the gas-bearing reservoir rock and forms the sole entry point for gas and brine into the wellbore. Brine was sampled in collaboration with RAG Austria AG Well Service using a particular sampling device (L: 4.42 m, V: 1.8 l), which was surface sterilized with steam and 70% ethanol and rinsed with sterile ultra-pure water before introduction into the wellbore. Brine samples from the reservoir were transferred into autoclaved gas-tight glass bottles (Pyrex) and purged with argon gas (5.0, Messer Austria GmbH) to create an oxygen-free atmosphere. Samples were stored in the dark, at ambient temperature (< 10 °C) during transport and processed within 12 hours after sampling.

Mesocosm set-up

High-pressure mesocosms with a working volume of 1.8 l each were manufactured from high-quality stainless steel (AISI 316 Ti) to prevent embrittlement, corrosion and gas losses. Online sensors monitored mesocosm pressure and temperature, maintained at 40 °C using an in-house designed control system. Supplementary Fig. 7 provides a construction scheme of the mesocosms, and Supplementary Note 3 lists a detailed description of mesocosm instrumentation. Drill cores were transferred into the mesocosms in a glovebox (MECA PLEX 6B 80) under an argon atmosphere (5.0, Messer Austria GmbH) with an oxygen concentration below 0.1% (v/v). The drill cores were flooded with brine sampled from the test reservoir to seed the mesocosms with autochthonous microorganisms. All mesocosms were pre-incubated for seven days at 40 °C before the initial substrate gas injection (constituting day 0). During the assembly of mesocosm 1 (M1), K_2HPO_4 was added to the brine to achieve a concentration of 0.22 mmol l^{-1}. No growth-assisting supplements were added to mesocosm 2 (M2), mesocosm 3 (M3), abiotic mesocosm 4 (M4) and abiotic mesocosm 5 (M5).

Elemental analysis of the reservoir brine (Supplementary Table 8) used for inoculation showed that essential trace elements for methanogens[62,63] (that is, nickel, molybdenum, zinc) were present naturally. In contrast, phosphate levels were below the limit of detection. The concentrations of the electron acceptors nitrate (NO_3^-) and sulfate (SO_4^{2-}) were negligible in reservoir brine (Supplementary Table 9).

A biocide (Grotan OX, Schülke and Mayr GmbH; 1% (v/v)) was added to the brine of abiotic mesocosms M4 and M5. After assembly (containing drill cores and reservoir brine), the abiotic control mesocosms were sterilized by γ-irradiation (35 kGy, MediScan GmbH and Co KG).

Mesocosm operation and sampling

Substrate gas was introduced into all mesocosms at a rate of approximately 2 bar min^{-1} from gas bottles containing 10% (v/v) of H_2 (5.0) and 2.5% (v/v) of CO_2 (4.5) in CH_4 (4.5) (±2% relative, Messer Austria GmbH) to a final pressure of approximately 40 bar. Variation in starting pressure is owed to a combination of technical constraints and manual operation and was compensated by normalizing values as described for headspace gas analysis. Abiotic control mesocosms were pressurized similarly to simulate the range of starting pressure variation in the biotic mesocosms from 39 to 45 bar. Pressure was monitored at intervals of 30 minutes in both biotic and abiotic mesocosms over the entire experimental period. Mesocosm liquid of M1, M2 and M3 was sampled before, during and after exposure to the substrate gas mixture. Supplementary Table 9 lists sampling time points. Supplementary Note 4 describes the chemical analysis of reservoir brine and mesocosm liquids in detail. Gas sampling was performed after each gas refill at the beginning of the new cycle and when the maximum pressure decrease was reached. Offline analysis of headspace gas components requires the removal of substantial amounts of gas, which reduces total mesocosm pressure and substrate available for microbial conversion. Therefore, intermediate gas sampling was only carried out in three cycles of M3. In total, 42 geo-methanation cycles were carried out in M3 and ten cycles were carried out in M1 and M2 each, with start and end-point sampling only.

Headspace gas analysis

Mesocosm headspace gas was analysed according to the method published by Rachbauer et al.[64]. Details on the employed two-stream gas chromatographic system are provided in Supplementary Note 5. Samples were collected from the mesocosms using evacuated 1 l gas bags (SUPEL Inert Foil Gasbags, article number 30227-U, Sigma-Aldrich), resulting in a pressure decrease of approximately 0.6 bar per sampling. The partial pressures of gas components (H_2, CO_2, CH_4) at the start ($P_{i\text{-}init}$) and end-point ($P_{i\text{-}end}$) of each gas conversion cycle were approximated using headspace gas concentrations (GC analysis) and total mesocosm pressure, assuming ideal behaviour due to the relatively low absolute pressure. Total mesocosm pressure was corrected for abiotic losses. Partial pressure change per cycle was calculated by subtracting $P_{i\text{-}init}$ from net $P_{i\text{-}end}$ using custom-made R code.

The ideal gas law was used to derive molar gas amounts from partial pressure data. The headspace volume was estimated from total mesocosm volume, the average effective porosity of 20.5% for all Sierning drill cores and liquid levels in the mesocosm at start and end time points, respectively. Gravimetric measurements of mesocosms determined liquid levels before and after the introduction of reservoir brine.

DNA isolation

Biomass in mesocosm fluid and reservoir brine (100 ml) was concentrated by membrane filtration (SuporR 200, 0.2 µm, ⌀ 47 mm, PALL Life Sciences). All filters were cut in half. DNA was isolated from each filter fragment using the phenol-chloroform extraction method (Supplementary Note 6).

RNA isolation and reverse transcription polymerase chain reaction

Samples of reservoir brine (n = 3, V: 80 ml) drawn at a measured depth of 1,200 during the production phase on day 244 were centrifuged at 16,000 g for 30 minutes at 4 °C (Centrifuge 5810, Eppendorf Austria GmbH). The resulting pellet was resuspended in 2 ml supernatant and transferred into a sterile 2 ml tube (LoBind, PCR-clean, Eppendorf Austria GmbH). The concentrate was centrifuged for 5 minutes at 10,000 g at 4 °C. The resulting pellet was resuspended in 0.5 ml of supernatant. To stabilize RNA, 1 ml of RNA ProSoil Lysis solution (MP Biomedicals GmbH) was added immediately after this biomass concentration procedure. RNA was isolated using the RNA ProSoil Direct kit (MP Biomedicals GmbH) and cleaned with the RNA ProSoil purification kit (MP Biomedicals GmbH). The RNA concentration was determined using the Qubit RNA HS Assay Kit in a Qubit 3 fluorometer (Invitrogen, Thermo Fisher Scientific). cDNA fragments were synthesized using the SuperScript III First-Strand Synthesis System for RT-PCR (LifeTech) with random hexamer priming according to the manufacturer's instructions. All sample manipulation steps were performed under anoxic conditions (O_2 < 0.1%).

Library preparation of *mcrA* mRNA isolated from reservoir brine

cDNA ('RNA isolation and RT-PCR') from total RNA extracts was used as a template in end-point polymerase chain reaction (PCR) to detect the expression of the *mcrA* gene in reservoir brine sampled during the production period of the field trial on day 244. The PCR programme was performed according to the method published by Munk et al.[65] using 2U Platinum Taq polymerase per reaction (LifeTech) and 5 µl of cDNA template. Next generation sequencing (NGS) libraries for the *mcrA*/*mrtA* locus were constructed using a nested PCR approach. The first PCR aimed to amplify the target sequence using the iMeA[62] primers iMeA_1046_F and iMeA_1435_R (Supplementary Table 10). The PCR product was purified with the NucleoSpin Gel and PCR Clean-up kit (Macherey–Nagel), and 2.5 µl of purified PCR product was used as a template in the second PCR[46] using the primers NGS_iMeA_1046F and NGS_iMeA_1435R (Supplementary Table 10).

16S library preparation and sequencing

NGS libraries were constructed from the V4-16S rRNA amplicons and sequenced as detailed in Supplementary Note 7. Primer sequences are listed in Supplementary Table 10.

Quality control of PCR reactions

PCR specificity was assessed by electrophoretic separation (10 V cm^{-1}) of PCR products on 1.5% agarose gels and ethidium bromide staining 1× Tris-acetate-EDTA (TAE) buffer made from ROTIPHORESE 50× TAE buffer. DNA and RNA isolates of *M. formicicum* strain *DSM 1535 T* were used as positive controls for all PCRs. The cultures of *M. formicicum* were grown to saturation in sterile 120 ml serum bottles in autoclaved, anoxic Klasson medium[66] at a pH of 7.0 pressurized to 3 bar as previously described[67] with a gas mixture containing 20% (v/v) CO_2 in H_2 (Air Liquide GmbH). Saturated cultures were submitted to DNA or RNA isolation.

Amplicon sequencing data processing

Trimmed 16S rRNA and *mcrA*/*mrtA* reads (fastq) were processed and analysed using the DADA2 software version 1.28[68]. Forward and reverse reads were quality filtered, allowing a maximum of two expected errors per read and a minimum quality of 2. Forward and reverse reads were truncated to 200 base pairs (bp) and 150 bp, respectively. ASVs were mapped against the SILVA SSU Ref NR 138.1 dataset[69]. *mcrA*/*mrtA* reads were subjected to a quality filtering step, removing reads with a maximum expected error <2. Forward and reverse reads were truncated at 245 bp and 200 bp, respectively, and were merged with a minimum overlap of 12 nucleotides, allowing 0 mismatches in the overlap region. The *mcrA* ASVs were mapped against the taxonomic *mcrA* gene database uploaded at GFZ Data Services.[70]

Quantitative analysis of geo-methanation

Quantitative geo-methanation results were inferred from time-dependent mesocosm pressure and headspace gas concentrations in M3. We included only cycles without intermediate headspace gas sampling with a total pressure greater than 39 bar and a run time of at least ten days (n = 14 out of 24) to ensure consistency. At a run time of ten days, we confidently determined the pressure plateau and verified the completion of the geo-methanation process. Pressure readings were corrected for pressure decrease observed in abiotic control mesocosms (M4, M5) to isolate pressure changes caused by microbial consumption of the introduced gases as opposed to abiotic effects. This corrected value, referred to as net pressure or corrected pressure was calculated by adding the pressure drop observed in the abiotic mesocosms (arithmetic mean of ten cycles operated at 40 bar target pressure) to the pressure reading obtained in M3 at the corresponding time point, normalized to starting pressure.

Stability metrics (maximum conversion rate, CR_{max} and pressure difference, Δp) were derived from 14 conversion cycles in mesocosm M3 with a minimum run time of ten days. CR_{max} for H_2 is defined as the minor time derivative inferred from the temporal development of normalized net pressure loss of each conversion cycle using the method published by Swain et al.[45]. Δp is defined as the pressure difference (net pressure loss) between the normalized starting pressure and the normalized final pressure at the end of each conversion cycle. It was calculated from Gauss-fitted data by subtracting the average pressure over the last six hours of each cycle ($t_{9.75} - t_{10}$) from 1 (t_0). CR_{max} and Δp were linearly regressed over time, applying the least squares regression method. The slope of the regression line was tested for significant differences from zero using F-Test statistics (GraphPad Prism version 10.1.1).

Methane evolution rate

Methane evolution rate (MER) is the molar amount of CH_4 produced per time interval (Δt) in a defined volume. It was calculated as described previously[52], according to equation (7). MER calculation was based on a stoichiometric gas mixture containing 10% H_2 and 2.5% CO_2 as used in mesocosm trials and the volume of reservoir brine (V_b) in the Lehen reservoir (40,000 m^3). The ideal gas law with a volume of 22.4 l mol^{-1} at standard temperature and pressure for any given gas was used to calculate the molar amount of methane (Δn_{CH_4}) to be produced from the injected gas.

$$\mathrm{MER}\ (\mathrm{mmol\ l^{-1}\ h^{-1}}) = \frac{\Delta n_{CH_4}}{\Delta t \times V_b} \tag{7}$$

The hypothetical overall capacity of the Lehen reservoir for geo-methanation was estimated in alignment with field trial parameters (operated gas volume (V_{TF}), CO_2 concentration of 2.5%) and assuming four gas conversion cycles per year and 95% conversion within 4.9 days (as reported for mesocosm trials).

$$\text{geo-methanation capacity}\ (\mathrm{m^3}) = V_{TF}\ (\mathrm{m^3}) \times \frac{0.95 \times CO_2\ (\%)}{100} \times 4\ \text{cycles} \tag{8}$$

Statistical analysis of CH_4 carbon isotope ratios

Differences between $\delta^{13}C_{CH4}$ values ($n = 2$) of gas samples taken during shut-in were determined using one-way ANOVA and Dunnet's post-hoc test, where the sample at the start of shut-in (day 96) was treated as the control group.

The difference between $\delta^{13}C_{CH4}$ values averaged over injection ($n = 11$) and extraction ($n = 5$) was tested for significance using the unpaired *t* test with Welch correction. All tests were accomplished using GraphPad Prism (version 10.1.1).

Data availability

The authors confirm that the data supporting the findings of this study are available within the article and supplementary information. In addition, source data files are provided for download. 16S rRNA gene and *mcrA* sequence data are available from the NCBI BioProject database (https://www.ncbi.nlm.nih.gov/bioproject) under study accession number PRJNA784117. Source data are provided with this paper.

Code availability

Custom-made R code for data analysis of field trial and laboratory-based mesocosm experiments is available from https://doi.org/10.5281/zenodo.10215007.

References

1. *Net Zero Roadmap: A Global Pathway to Keep the 1.5 °C Goal in Reach* (IEA, 2023); https://www.iea.org/reports/net-zero-roadmap-a-global-pathway-to-keep-the-15-0c-goal-in-reach
2. Sinsel, S. R., Riemke, R. L. & Hoffmann, V. H. Challenges and solution technologies for the integration of variable renewable energy sources—a review. *Renew. Energy* **145**, 2271–2285 (2020).
3. Pacesila, M., Burcea, S. G. & Colesca, S. E. Analysis of renewable energies in European Union. *Renew. Sustain. Energy Rev.* **56**, 156–170 (2016).
4. Gür, T. M. Review of electrical energy storage technologies, materials, and systems: challenges and prospects for large-scale grid storage. *Energy Environ. Sci.* **11**, 2696–2767 (2018).
5. Luo, X., Wang, J., Dooner, M. & Clarke, J. Overview of current development in electrical energy storage technologies and the application potential in power system operation. *Appl. Energy* **137**, 511–536 (2015).
6. Lehner, M., Tichler, R., Steinmüller, H. & Koppe, M. *Power-to-Gas: Technology and Business Models. SpringerBriefs in Energy* (Springer, 2014).
7. Götz, M. et al. Renewable power-to-gas: a technological and economic review. *Renew. Energy* **85**, 1371–1390 (2016).
8. Wulf, C., Linssen, J. & Zapp, P. in *Hydrogen Supply Chain: Design, Deployment and Operation* (ed. Azzaro-Pantel, C.) 309–345 (Academic Press, 2018).
9. Panchenko, V. A., Daus, Y. V., Kovalev, A. A., Yudaev, I. V. & Litti, Y. V. Prospects for the production of green hydrogen: review of countries with high potential. *Int. J. Hydrogen Energy* **48**, 4551–4571 (2023).
10. Lazar, M. D., Mihet, M. & Dan, M. in *Comprehensive Renewable Energy* 2nd edn (ed. Letcher, T. M.) 553–565 (Elsevier, 2022).
11. Denholm, P. & Mai, T. Timescales of energy storage needed for reducing renewable energy curtailment. *Renew. Energy* **130**, 388–399 (2019).
12. Heinemann, N. et al. Enabling large-scale hydrogen storage in porous media—the scientific challenges. *Energy Environ. Sci.* **14**, 853–864 (2021).
13. Carden, P. O. & Paterson, L. Physical, chemical and energy aspects of underground hydrogen storage. *Int. J. Hydrogen Energy* **4**, 559–569 (1979).
14. Šmigáň, P. et al. Methanogenic bacteria as a key factor involved in changes of town gas stored in an underground reservoir. *FEMS Microbiol. Lett.* **73**, 221–224 (1990).
15. Crotogino, F. in *Storing Energy: with Special Reference to Renewable Energy Sources* (ed. Letcher, T.) 613–632 (Elsevier, 2022).
16. Panfilov, M. in *Compendium of Hydrogen Energy* (eds Gupta, R. B., Basile A. & Veziroğlu, T. N.) 91–115 (Woodhead Publishing, 2016).
17. *Transporting Pure Hydrogen by Repurposing Existing Gas Infrastructure: Overview of Existing Studies and Reflections on the Conditions for Repurposing* (ACER, 2021).
18. Thaysen, E. M. et al. Estimating microbial growth and hydrogen consumption in hydrogen storage in porous media. *Renew. Sustain. Energy Rev.* **151**, 111481 (2021).
19. Buriánková, I. et al. Microbial communities in underground gas reservoirs offer promising biotechnological potential. *Fermentation* **8**, 251 (2022).
20. Zauner, A. et al. Multidisciplinary assessment of a novel carbon capture and utilization concept including underground sun conversion. *Energies* **15**, 1021 (2022).
21. Lee, S. W., Lee, H. S., Park, Y. J. & Cho, Y. S. Combustion and emission characteristics of HCNG in a constant volume chamber. *J. Mech. Sci. Technol.* **25**, 489–494 (2011).
22. Strobel, G., Hagemann, B., Huppertz, T. M. & Ganzer, L. Underground bio-methanation: concept and potential. *Renew. Sustain. Energy Rev.* **123**, 109747 (2020).
23. Robinson, N. P. & Buan, N. R. Methanogens: pushing the boundaries of biology. *Emerging Top. Life Sci.* **2**, 629–646 (2018).
24. Gray, N., O'Shea, R., Smyth, B., Lens, P. N. L. & Murphy, J. D. What is the energy balance of electrofuels produced through power-to-fuel integration with biogas facilities? *Renew. Sustain. Energy Rev.* **155**, 111886 (2022).
25. Mendoza-Hernandez, O. S. et al. Exergy valorization of a water electrolyzer and CO_2 hydrogenation tandem system for hydrogen and methane production. *Sci. Rep.* **9**, 6470 (2019).
26. Brooks, K. P., Hu, J., Zhu, H. & Kee, R. J. Methanation of carbon dioxide by hydrogen reduction using the Sabatier process in microchannel reactors. *Chem. Eng. Sci.* **62**, 1161–1170 (2007).
27. Lyu, Z., Shao, N., Akinyemi, T. & Whitman, W. B. Methanogenesis. *Curr. Biol.* **28**, R727–R732 (2018).
28. Zabranska, J. & Pokorna, D. Bioconversion of carbon dioxide to methane using hydrogen and hydrogenotrophic methanogens. *Biotechnol. Adv.* **36**, 707–720 (2018).
29. Contreras, G. et al. New perspectives for biotechnological applications of methanogens. *Curr. Res. Biotechnol.* **4**, 468–474 (2022).
30. Schwartz, E. & Friedrich, B. in *The Prokaryotes: Volume 2: Ecophysiology and Biochemistry* (eds Dworkin, M. et al.) 496–563 (Springer, 2006).
31. Weijma, J. et al. Competition for H_2 between sulfate reducers, methanogens and homoacetogens in a gas-lift reactor. *Water Sci. Technol.* **45**, 75–80 (2002).
32. Muyzer, G. & Stams, A. J. M. The ecology and biotechnology of sulphate-reducing bacteria. *Nat. Rev. Microbiol.* **6**, 441–454 (2008).
33. Jiang, G., Keller, J. & Bond, P. L. Determining the long-term effects of H_2S concentration, relative humidity and air temperature on concrete sewer corrosion. *Water Res.* **65**, 157–169 (2014).
34. *Underground Sun Storage: Final Report Public* (RAG Austria AG, 2017); https://www.underground-sun-storage.at/en/public-relations-/-publications/publications-1.html
35. Meister, S. in *Underground Storage of Natural Gas: Theory and Practice* (ed. Tek, M. R.) 387–403 (Springer Netherlands, 1989).
36. Chabab, S., Théveneau, P., Coquelet, C., Corvisier, J. & Paricaud, P. Measurements and predictive models of high-pressure H_2 solubility in brine (H_2O+NaCl) for underground hydrogen storage application. *Int. J. Hydrog. Energy* **45**, 32206–32220 (2020).

37. Hassanpouryouzband, A. et al. Geological hydrogen storage: geochemical reactivity of hydrogen with sandstone reservoirs. *ACS Energy Lett.* **7**, 2203–2210 (2022).
38. Yekta, A. E., Pichavant, M. & Audigane, P. Evaluation of geochemical reactivity of hydrogen in sandstone: application to geological storage. *Appl. Geochem.* **95**, 182–194 (2018).
39. Truche, L. et al. Sulphide mineral reactions in clay-rich rock induced by high hydrogen pressure. Application to disturbed or natural settings up to 250 °C and 30 bar. *Chem. Geol.* **351**, 217–228 (2013).
40. Hattori, S. Syntrophic acetate-oxidizing microbes in methanogenic environments. *Microbes Environ.* **23**, 118–127 (2008).
41. Westerholm, M., Roos, S. & Schnürer, A. *Syntrophaceticus schinkii* gen. nov., sp. nov., an anaerobic, syntrophic acetate-oxidizing bacterium isolated from a mesophilic anaerobic filter. *FEMS Microbiol. Lett.* **309**, 100–104 (2010).
42. Parshina, S. N. et al. *Soehngenia saccharolytica* gen. nov., sp. nov. and *Clostridium amygdalinum* sp. nov., two novel anaerobic, benzaldehyde-converting bacteria. *Int. J. Syst. Evol. Microbiol.* **53**, 1791–1799 (2003).
43. Nazina, T. N. et al. *Soehngenia longivitae* sp. nov., a fermenting bacterium isolated from a petroleum reservoir in Azerbaijan, and emended description of the genus *Soehngenia*. *Microorganisms* **8**, 1967 (2020).
44. Liu, Y.-F. et al. Anaerobic hydrocarbon degradation in candidate phylum 'Atribacteria' (JS1) inferred from genomics. *ISME J.* **13**, 2377–2390 (2019).
45. Sleat, R., Mah, R. A. & Robinson, R. *Acetoanaerobium noterae* gen. nov., sp. nov.: an anaerobic bacterium that forms acetate from H_2 and CO_2. *Int. J. Syst. Evol. Microbiol.* **35**, 10–15 (1985).
46. Bauer, C., Korthals, M., Gronauer, A. & Lebuhn, M. Methanogens in biogas production from renewable resources—a novel molecular population analysis approach. *Water Sci. Technol.* **58**, 1433–1439 (2008).
47. Morris, R. et al. Methyl coenzyme M reductase (mcrA) gene abundance correlates with activity measurements of methanogenic H_2/CO_2-enriched anaerobic biomass. *Microb. Biotechnol.* **7**, 77–84 (2014).
48. Tyne, R. L. et al. Rapid microbial methanogenesis during CO_2 storage in hydrocarbon reservoirs. *Nature* **600**, 670–674 (2021).
49. Coplen, T. B. Guidelines and recommended terms for expression of stable-isotope-ratio and gas-ratio measurement results. *Rapid Commun. Mass Spectrom.* **25**, 2538–2560 (2011).
50. Swain, P. S. et al. Inferring time derivatives including cell growth rates using Gaussian processes. *Nat. Commun.* **7**, 13766 (2016).
51. Taubner, R. S. et al. Biological methane production under putative Enceladus-like conditions. *Nat. Commun.* **9**, 748 (2018).
52. Pappenreiter, P. A., Zwirtmayr, S., Mauerhofer, L.-M., Rittmann, S. K.-M. R. & Paulik, C. Development of a simultaneous bioreactor system for characterization of gas production kinetics of methanogenic archaea at high pressure. *Eng. Life Sci.* **19**, 537–544 (2019).
53. Cheng, L., Dai, L., Li, X., Zhang, H. & Lu, Y. Isolation and characterization of *Methanothermobacter crinale* sp. nov., a novel hydrogenotrophic methanogen from the Shengli oil field. *Appl. Environ. Microbiol.* **77**, 5212–5219 (2011).
54. Hassa, J., Wibberg, D., Maus, I., Pühler, A. & Schlüter, A. Genome analyses and genome-centered metatranscriptomics of *Methanothermobacter wolfeiiStrain* SIV6, isolated from a thermophilic production-scale biogas fermenter. *Microorganisms* **8**, 13 (2019).
55. Dabir, A. et al. Draft genome sequence of *Methanoculleus* sp. MH98A, a novel methanogen isolated from sub-seafloor methane hydrate deposits in Krishna Godavari basin. *Mar. Genomics* **18PB**, 139–140 (2014).
56. Hogeweg, S., Hagemann, B. & Ganzer, L. Simulation of freshwater injection to enable underground bio-methanation in high-saline gas storage formations. In *EAGE GET 2022* Vol. 2022, 1–5 (European Association of Geoscientists & Engineers, 2022).
57. Khajooie, S., Gaus, G., Dohrmann, A. B., Krüger, M. & Littke, R. Methanogenic conversion of hydrogen to methane in reservoir rocks: an experimental study of microbial activity in water-filled pore space. *Int. J. Hydrog. Energy* **50**, 272–290 (2024).
58. Bouteldja, M. et al. *Definition of Selection Criteria for a Hydrogen Storage Site in Depleted Fields or Aquifers* (INIS-FR–22-0496) (INIS, 2021).
59. Schulz, H., Berk, W. V., Bechtel, A., Struck, U. & Faber, E. Bacterial methane in the Atzbach-Schwanenstadt gas field (Upper Austrian Molasse Basin), part I: geology. *Mar. Pet. Geol.* **26**, 1163–1179 (2009).
60. Andrews, J. N., Youngman, M. J., Goldbrunner, J. E. & Darling, W. G. The geochemistry of formation waters in the molasse basin of upper Austria. *Environ. Geol. Water Sci.* **10**, 43–57 (1987).
61. Fetkovich, M. J., Fetkovich, E. J. & Fetkovich, M. D. Useful concepts for decline-curve forecasting, reserve estimation, and analysis. *SPE Reservoir Eng.* **11**, 13–22 (1996).
62. Rosenwinkel, K.-H., Kroiss, H., Dichtl, N., Seyfried, C.-F. & Weiland, P. *Anaerobtechnik* (Springer Vieweg, 2015).
63. Jarrell, K. F. & Kalmokoff, M. L. Nutritional requirements of the methanogenic archaebacteria. *Can. J. Microbiol.* **34**, 557–576 (1988).
64. Rachbauer, L., Voitl, G., Bochmann, G. & Fuchs, W. Biological biogas upgrading capacity of a hydrogenotrophic community in a trickle-bed reactor. *Appl. Energy* **180**, 483–490 (2016).
65. Munk, B., Bauer, C., Gronauer, A. & Lebuhn, M. Population dynamics of methanogens during acidification of biogas fermenters fed with maize silage. *Eng. Life Sci.* **10**, 496–508 (2010).
66. Klasson, K. T. et al. Methane production from synthesis gas using a mixed culture of *R. rubrum M. barkeri*, and *M. formicicum*. *Appl. Biochem. Biotechnol.* **24–25**, 317–328 (1990).
67. Taubner, R. S. & Rittmann, S. K. M. R. Method for indirect quantification of CH_4 production via H_2O production using hydrogenotrophic methanogens. *Front. Microbiol.* **7**, 532 (2016).
68. Callahan, B. J. et al. DADA2: high-resolution sample inference from Illumina amplicon data. *Nat. Methods* **13**, 581–583 (2016).
69. Quast, C. et al. The SILVA ribosomal RNA gene database project: improved data processing and web-based tools. *Nucleic Acids Res.* **41**, D590–D596 (2013).
70. Yang, S., Liebner, S., Alawi, M., Ebenhöh, O. & Wagner, D. Taxonomic database and cut-off value for processing *mcrA* gene 454 pyrosequencing data by MOTHUR. *J. Microbiol. Methods* **103**, 3–5 (2014).

Acknowledgements

This study is based on research accomplished within the flagship projects Underground Sun Storage (number 840705) and Underground Sun Conversion (number 855231), both funded by the Austrian Climate and Energy Fund and the Austrian Research Promotion Agency (FFG). The authors thank Ł. Chrzanowski for carefully revising the manuscript.

Author contributions

Conceptualization: S.B., C.H., A.P.L., M.P., L.R., J.S. and A.B.Z. Experimental work: A.A., C.H., M.P., J.S. and N.W. Project planning: S.B., C.H., A.P.L., M.P., J.S. and N.W. Data analysis: A.A., C.H., A.P.L., M.P., L.R., K.E.S., J.S., N.W. and A.B.Z. Writing of the manuscript: C.H., A.P.L., M.P., L.R., K.E.S., N.W. and A. Z.

Competing interests

S.B., M.P., A.P.L., J.S. and K.E.S. are listed as inventors on a patent filed by RAG Austria AG on the development of a method for hydrogenotrophic

methanogenesis in exploited reservoirs (EP 3 280 807 B1, 2015-03-26 priority, 2019-10-09 application granted). S.B., M.P. and A.A. are employed at RAG Austria AG. All other authors declare no competing interests.

Additional information

Supplementary information The online version contains supplementary material available at https://doi.org/10.1038/s41560-024-01458-1.

Correspondence and requests for materials should be addressed to Andreas P. Loibner.

Peer review information *Nature Energy* thanks Elliott Barnhart, Gion Strobel and Marc Strous for their contribution to the peer review of this work.